Study of regular and irregular states in generic systems

1999 J. Phys. A: Math. Gen. 32 6423

(http://iopscience.iop.org/0305-4470/32/36/306)

J. Phys. A: Math. Gen. **32** (1999) 6423–6444. Printed in the UK PII: S0305-4470(99)03256-4

Study of regular and irregular states in generic systems

Gregor Veble, Marko Robnik and Junxian Liu

Center for Applied Mathematics and Theoretical Physics, University of Maribor, Krekova 2, SI–2000 Maribor, Slovenia

E-mail: robnik@uni-mb.si, gregor.veble@uni-mb.si and junxian.liu@uni-mb.si

Received 8 April 1999

Abstract. In this work we present the results of a numerical and semiclassical analysis of high-lying states in a Hamiltonian system, whose classical mechanics is of a generic, mixed type, where the energy surface is split into regions of regular and chaotic motion. As predicted by the principle of uniform semiclassical condensation, when the effective $\hbar$ tends to zero, each state can be classified as regular or irregular. We were able to semiclassically reproduce individual regular states by the Einstein–Brillouin–Keller torus quantization, for which we devise a new approach, while for the irregular ones we found the semiclassical prediction of their autocorrelation function, in a good agreement with numerics. We also looked at the low-lying states to get a better understanding of the onset of semiclassical behaviour.

1. Introduction

There is a remarkable difference between the quantum properties of the classically integrable and fully chaotic (ergodic) systems. While in the integrable case the wavefunctions possess an ordered structure, the eigenstates of classically ergodic systems appear random (Berry 1977, Voros 1979) in the semiclassical limit $\hbar \to 0$. They can be well represented locally as a superposition of plane waves with equal wavevector magnitude but random phases, leading to the Gaussian distribution of the wavefunction amplitude. The assumption of random phases may, however, break down on dynamical grounds when $\hbar$ is insufficiently small. This leads to the phenomenon of scars, which are the regions of amplified wavefunction amplitude close to the short and weakly unstable classical periodic orbits (Heller 1984).

In the classically mixed systems the energy (hyper)surface is split into both chaotic regions, within which the motion is ergodic, and the regular regions where motion is, as in the fully integrable case, quasiperiodic and confined to invariant tori within the energy surface. We call such systems generic since this is the most general type of Hamiltonian dynamics. The principle of uniform semiclassical condensation (PUSC) (see Robnik 1988, 1998) states that the quantal phase space distribution of any eigenstate, given by its Wigner function, should be uniformly distributed on a classically invariant object in the phase space when $\hbar \to 0$. This object can be either an invariant torus in one of the regular regions in the phase space or a whole chaotic component.

While the PUSC is valid for fully integrable and ergodic systems, its full potential is shown when applied to the generic case. Here it predicts that the eigenstates are separated into regular and irregular ones, depending on whether the classical object onto which their Wigner function condenses is a regular torus or a chaotic component, respectively. This has far-reaching consequences leading, for example, to the picture of Berry and Robnik (1984) for

0305-4470/99/366423+22$30.00

the statistics of energy levels, where the regular and chaotic states are assumed to contribute independent level sequences to the total spectrum. This was confirmed by many numerical computations (Prosen and Robnik 1993b, 1994, 1999, Prosen 1995, 1996, 1998, Robnik 1998).

In this work we are interested in geometrical and statistical properties of high-lying eigenfunctions. It is an extension of previous work done on mixed-type systems by Prosen and Robnik (1993c, 1994) and by Li and Robnik (1995a, b), but also relates to and further develops the paper by Li and Robnik (1994) concerning the statistical properties of chaotic states, which differ drastically from the properties of regular states in classically integrable systems (Robnik and Veble 1998). The main step forward in the numerical direction is the use of the so-called scaling method, introduced by Vergini and Saraceno (1995), with which we have obtained the states with consecutive indices around 2.5×10^6, thus enabling us to go much farther into the semiclassical region. On the other hand, we have been able to semiclassically reconstruct the numerically obtained regular states by employing the Einstein–Brillouin–Keller (EBK) torus quantization in section 3.1, where we offer a new approach to this problem, especially on the numerical side. While we were not able to semiclassically reconstruct the chaotic states, we obtained a good prediction of their statistical properties by strictly employing the PUSC (see Robnik 1998) in section 3.2.

2. Our catalogues of states

We dealt with a model billiard system obtained by conformally mapping the unit circle with the complex quadratic polynomial, as introduced by Robnik (1983, 1984),

$$z \to w(z) = z + \lambda z^2 \qquad w(z) = x + \mathrm{i}y. \tag{1}$$

The range of x at $y = 0$ inside the billiard is $x \in [-1 + \lambda, +1 + \lambda]$. We used the value of $\lambda = 0.15$, where the classical phase space is roughly divided into equal components of regular and chaotic motion. We chose the Poincaré surface of section (SOS) to lie on the symmetry axis $y = 0$ with coordinate x and the conjugate momentum p_x as the parameters of the surface. The intersection of the main chaotic component of our billiard with the SOS is shown in figure 1. The coordinate x is taken *relative to the centre of the billiard* (i.e. it is shifted by λ w.r.t. $x = 0$ of equation (1), so that now the range of x is $x \in [-1, +1]$), while p_x is the x-component of the unit momentum vector.

The quantum mechanics of billiards is described by the Helmholtz equation

$$(\Delta + k^2)\psi = 0 \tag{2}$$

with the Dirichlet boundary conditions, where $k^2 = 2mE/\hbar^2$. We limited ourselves to the states with even parity with respect to reflection across the symmetry line $y = 0$.

For each state we calculated the smoothed projection of the Wigner function. The Wigner function of a state $\psi(\boldsymbol{q})$ in the general case of N degrees of freedom is defined in the full phase space $(\boldsymbol{q}, \boldsymbol{p})$ as (Berry 1983)

$$W(\boldsymbol{q}, \boldsymbol{p}) = \frac{1}{(2\pi\hbar)^N} \int \mathrm{d}^N \boldsymbol{X}\ \exp(-\mathrm{i}\boldsymbol{p} \cdot \boldsymbol{X}/\hbar)\psi^\dagger(\boldsymbol{q} - \boldsymbol{X}/2)\psi(\boldsymbol{q} + \boldsymbol{X}/2). \tag{3}$$

In our case the eigenfunctions $\psi(x, y)$ generate their Wigner transforms $W(x, y, p_x, p_y)$ through (3), where $N = 2$. In order to compare the Wigner function of a state of our system with the classical SOS plot we took its value on the symmetry line ($y = 0$) and integrated it over p_y:

$$\rho_{SOS}(x, p_x) = \int \mathrm{d}p_y\, W(x, y = 0, p_x, p_y). \tag{4}$$

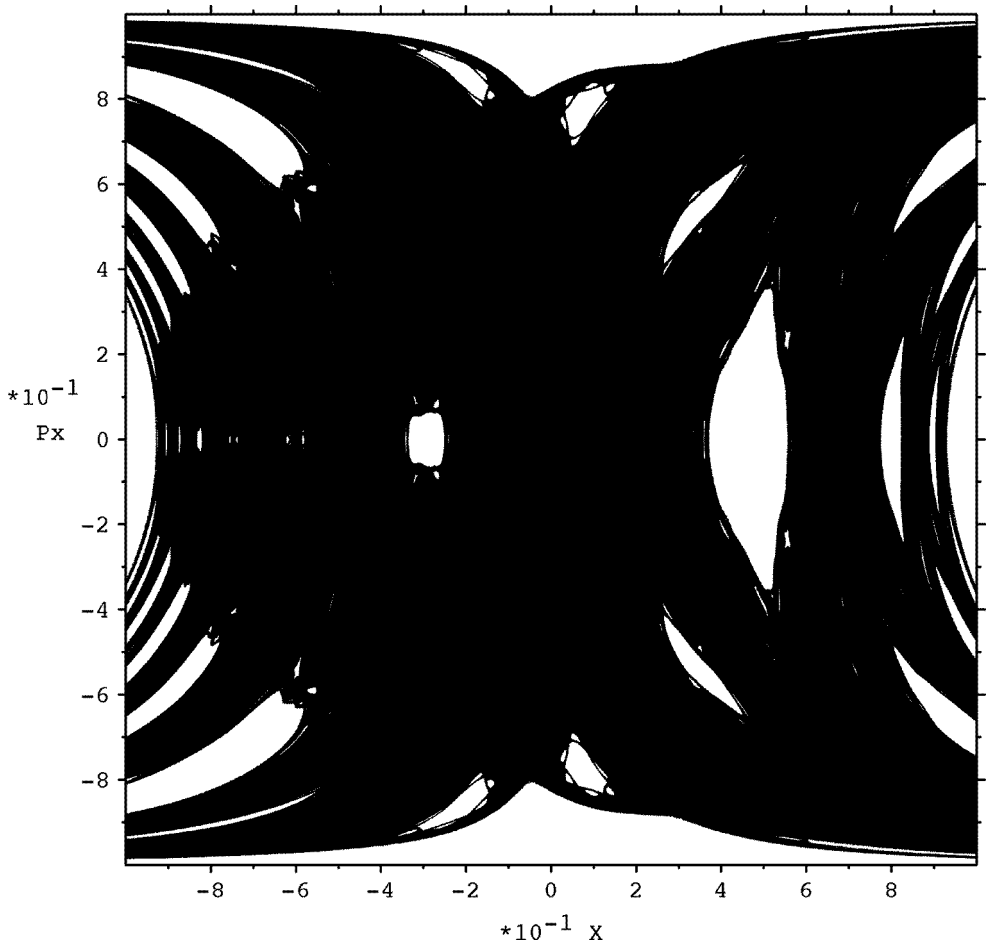

Figure 1. The SOS section of the main chaotic component of the $\lambda = 0.15$ billiard. The x coordinate here is shifted by λ to the right so that $x \in [-1, +1]$, and $x = 0$ corresponds to $x = \lambda$ of equation (1).

The result is

$$\rho_{SOS}(x, p_x) = \frac{1}{2\pi\hbar} \int \mathrm{d}X \ \exp(-\mathrm{i}p_x X/\hbar)\psi^{\dagger}(x - X/2, y = 0)\psi(x + X/2, y = 0). \qquad (5)$$

Here we see the reason for only considering the even parity states: because $\psi(x, y = 0)$ is exactly zero for odd states, we therefore require a different approach to analyse them.

As is well known, the Wigner function is not positive definite but exhibits small oscillations that can blur the overall picture. We chose to smooth the projection of the Wigner function by a suitable Gaussian. It was chosen narrower than the minimum uncertainty Gaussian (in which case the Wigner function becomes the positive definite Husimi distribution) in order to avoid smoothing out too many features, but still wide enough to reduce the oscillations.

The first catalogue of eigenstates and the corresponding smoothed Wigner function projections comprises the first 1000 even states. They were obtained by the conformal mapping diagonalization technique (as described in Robnik 1984). We stress that by this method no levels and eigenstates were lost, as can happen with other approaches such as Heller's plane

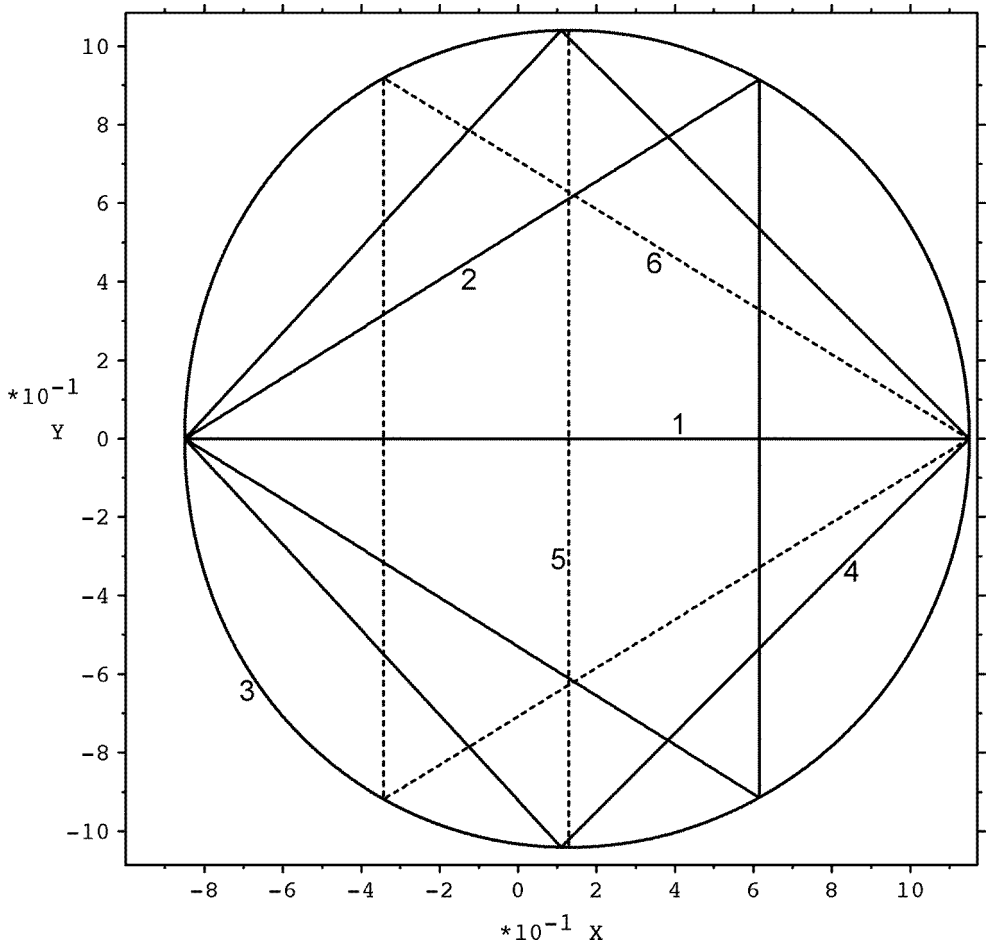

Figure 2. The shortest periodic orbits of the $\lambda = 0.15$ billiard (explained in text). The stable orbits are shown with full lines and the unstable ones with dashed lines.

wave decomposition method (Heller 1984) and/or the boundary integral method (see e.g. Berry and Wilkinson 1984) etc.

Such a complete catalogue gives us a good picture of the overall behaviour of the system. Many of the states in this low-energy region can be associated with the shortest classical periodic orbits. In a mixed-type system such as ours, there are both stable orbits that are found within the islands of stability, or unstable ones that lie within one of the chaotic components.

The shortest periodic orbits of our system are shown in figure 2. These are the stable (labelled by 1) and unstable (5) periodic orbits with two bounces, the stable (2) and unstable (6) three-bounce periodic orbits and the stable periodic orbit with four bounces (4). As our billiard is convex, there also exists an infinite number of stable periodic orbits skipping along the boundary (3) of the billiard, which are associated with and support the whispering gallery modes (Lazutkin 1981, 1991, Li and Robnik 1995a).

Examples of the states that correspond to the stable periodic orbits labelled 1–4 in figure 2 are shown in figure 3 with the smoothed projections of their Wigner functions shown in figure 5. Each row shows the states of the same type with increasing energy. The states corresponding to

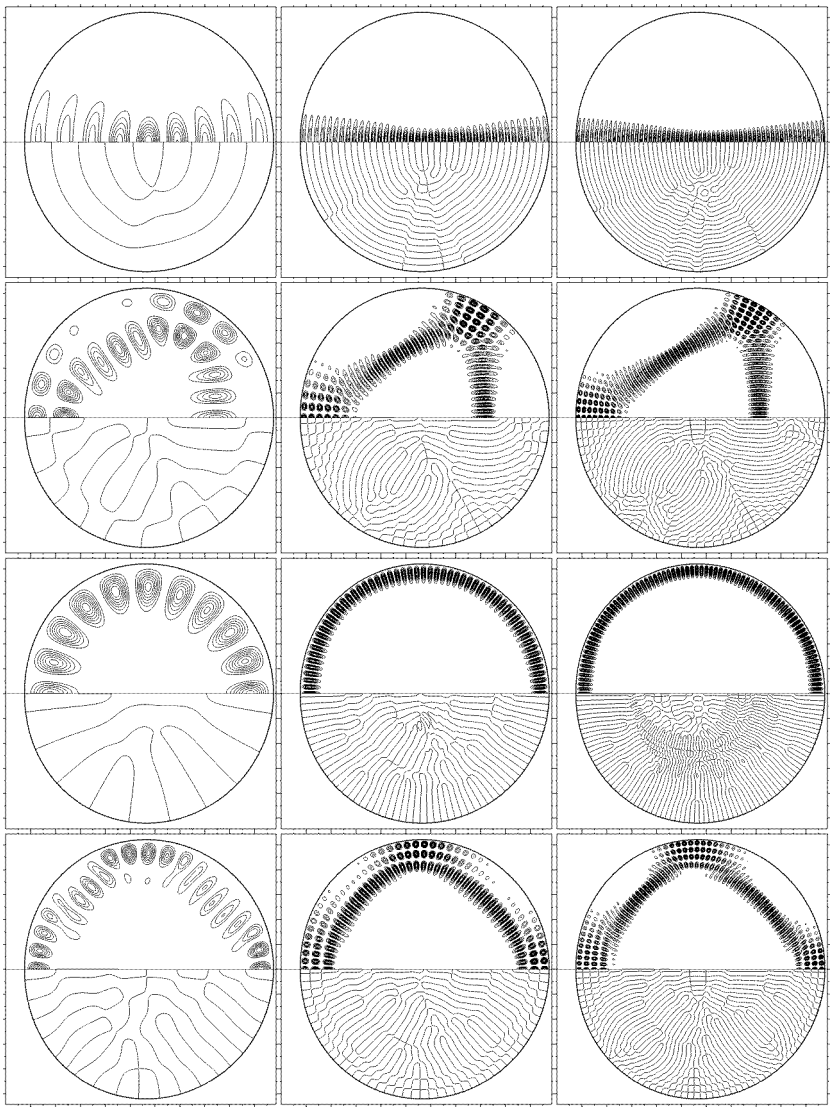

Figure 3. A selection of eigenstates corresponding to the stable periodic orbits 1–4 in figure 2 from top to bottom, respectively. In the top half of each plot we show the eight equally spaced contours of the probability density from zero to its maximum value. In the bottom half we show the nodal lines of each wavefunction.

the stable periodic orbits appear consistently and systematically across the catalogue of states. As we see later, they can be attributed to the quantized tori in the regular regions, and can be found for those tori whose actions satisfy the EBK quantization condition (see Robnik 1998). If we compare the Wigner plots of these states with the SOS plot in figure 1, we notice that the areas of greatest intensities of Wigner functions are found within the corresponding islands of stability in the SOS plot.

The states that correspond to the unstable periodic orbits with indices (5) and (6) are shown in the rows of figure 4 with the corresponding smoothed projections of their Wigner

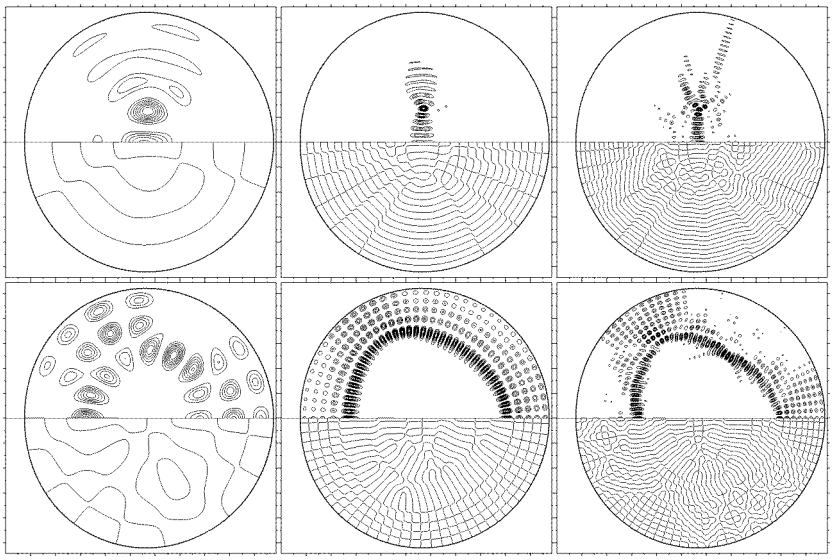

Figure 4. A selection of eigenstates corresponding to the stable periodic orbits 5 and 6 in figure 2 in the top and bottom row, respectively. In the top half of each plot we show the eight equally spaced contours of the probability density from zero to its maximum value. In the bottom half we show the nodal lines of each wavefunction.

functions given in figure 6, with their energy again increasing along the rows. The states corresponding to the unstable periodic orbits emerge with varying intensities with respect to the background, and are less frequent with increasing energy. The approximate position of their emergence in the spectrum can be determined by the condition that the classical action along the periodic orbit should be a multiple of Planck's constant plus the Maslov phase corrections due to the caustics formed by nearby trajectories (Robnik 1989). Therefore, in two-dimensional billiards, the intervals (either in energy E or the cumulative number of states $\mathcal{N}$) of consecutive re-appearance of the eigenstates of the same type grow as the square root of E or $\mathcal{N}$. Such states with increased intensities of amplitude close to the classically unstable periodic orbits are called scars (Heller 1984, 1986, Bogomolny 1988).

With increasing energy the longer periodic orbits start to manifest themselves in the structure of eigenstates; however, many of the states become increasingly difficult to associate with simple periodic orbits. Two examples of such states are shown in figure 7. The left state is a regular state spanned by a torus in the neighbourhood of the stable periodic orbit with three bounces, characterized by two quantum numbers. It is interesting to note that while the quantum number along the direction of the periodic orbit is quite large (about 140), the transversal quantum number is equal to one, giving rise to a single nodal line along the direction of the periodic orbit. On the other hand, the state on the right cannot be associated with only a single unstable periodic orbit, but instead with a large portion of the chaotic component, this being more prominent in the smoothed projections of the corresponding Wigner function shown in the lower row of figure 7.

The separation of states into regular and irregular ones becomes fully explicit in our second catalogue of states. The catalogue consists of 100 consecutive states starting at the consecutive index of about 2.5×10^6. These states were obtained by the scaling method first introduced by Vergini and Saraceno (1995), which enables us to find a few states in the neighbourhood of a chosen wavenumber k. As this is a diagonalizational method no levels were missed. Almost

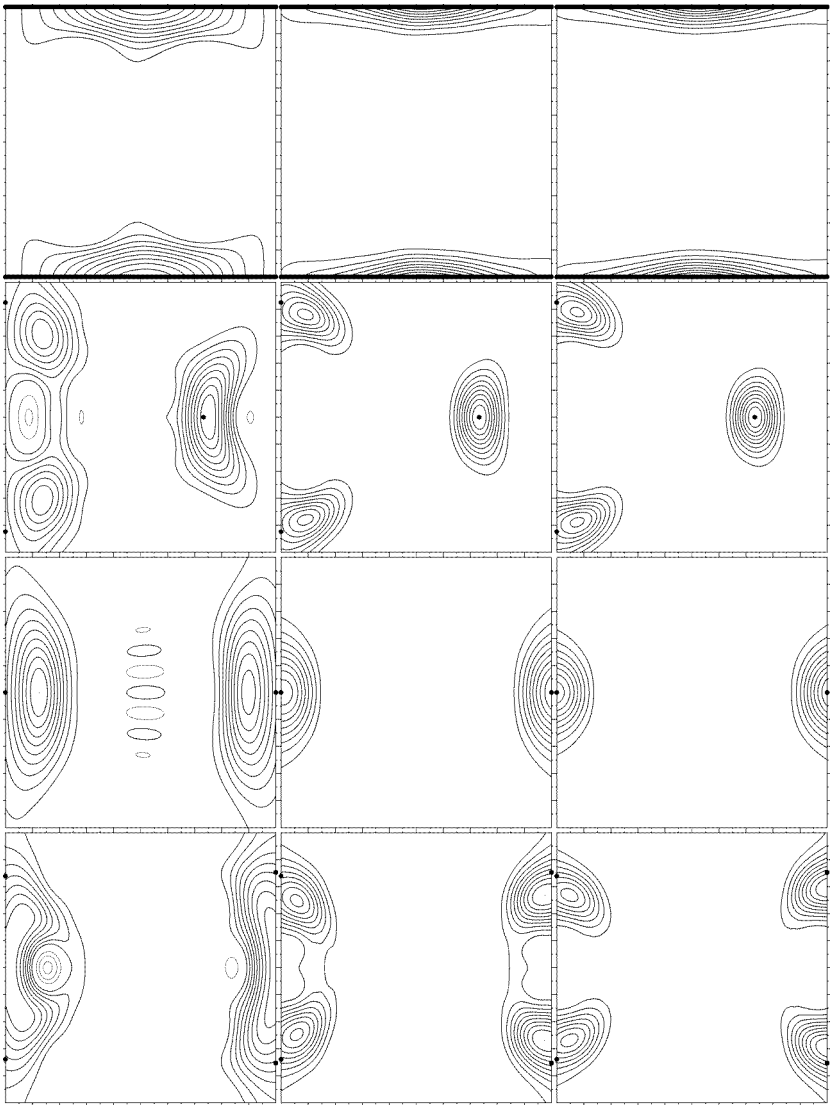

Figure 5. The corresponding smoothed projections of the Wigner functions for the wavefunctions in figure 3. The contours are spaced in ten intervals from zero to the maximal value. The negative value contours are plotted at the same spacing but with thinner lines. We do not plot the zero-level contour due to many oscillations of the Wigner functions when it is close to zero. As in all subsequent Wigner plots, the momentum p_x is measured in units of p', which is related to the energy of the eigenstate by $E = p'^2$. The locations of the relevant classical periodic orbits are marked by the 'bullets'. The x coordinate here is shifted by λ as in figure 1.

every level in our small catalogue can be clearly identified as regular or irregular, an idea already proposed by Percival (1973). The only exception in the catalogue is a pair of states lying close together with respect to the mean level spacing, shown in figure 8, where both of the states are superpositions of a regular ($|\psi_r\rangle$) and irregular ($|\psi_i\rangle$) state. These two states are close to a degeneracy of two energetically equal but structurally different quantized classical objects.

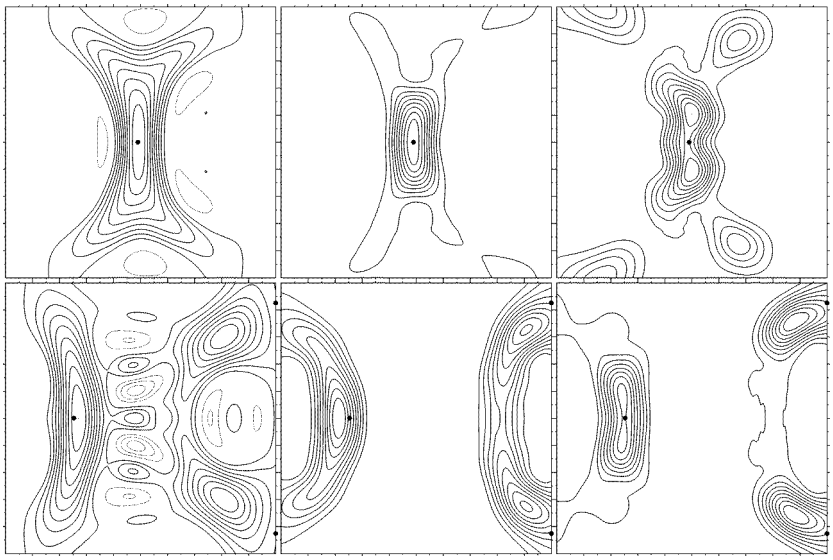

Figure 6. The corresponding smoothed projections of the Wigner functions for the wavefunctions in figure 4. The plotting method is the same as in figure 5.

This mixing is the consequence of the fact that the regular and irregular state are not exact solutions of the Hamiltonian which leads to the matrix element

$$H_{ri} = \langle \psi_r | \hat{H} | \psi_i \rangle \tag{6}$$

not being equal to zero. When two such states, or, more precisely, their adiabatically corresponding states, are brought close together on the energy scale by varying a parameter of the system (e.g. λ in our billiard), their eigenenergies do not cross but show a phenomenon of level repulsion (avoided crossing). In the cases when the effect of other levels can be neglected, the smallest energy spacing between the two levels reached is twice the value of the matrix element (6). At this point the eigenstates are exactly the symmetric and antisymmetric superpositions of the well-separated states. If we vary the parameter of the system further, the adiabatic equivalents of the original states will exchange identities.

While the avoided level crossings are typical for irregular states, the regular states do not exhibit the phenomenon of level repulsion amongst themselves (Berry 1983), except, possibly, on an exponentially small scale (due to the tunnelling effects). Furthermore, according to the PUSC, there should be no level repulsion between the regular and irregular states as $\overline{h} \to 0$. As this repulsion is directly connected to the mixing of states, the relative number of mixed states, such as the pair shown in figure 8, is expected to tend to zero when the effective Planck constant of the system tends to zero.

More states of both the regular and irregular type from this catalogue with their appropriate analysis are shown in the next section.

3. Analysis of states

The main purpose of our work was to understand to what extent it is possible to describe the structure of individual eigenstates by semiclassical methods. For completely integrable systems there exists the EBK method of torus quantization (see, for example, Berry 1983,

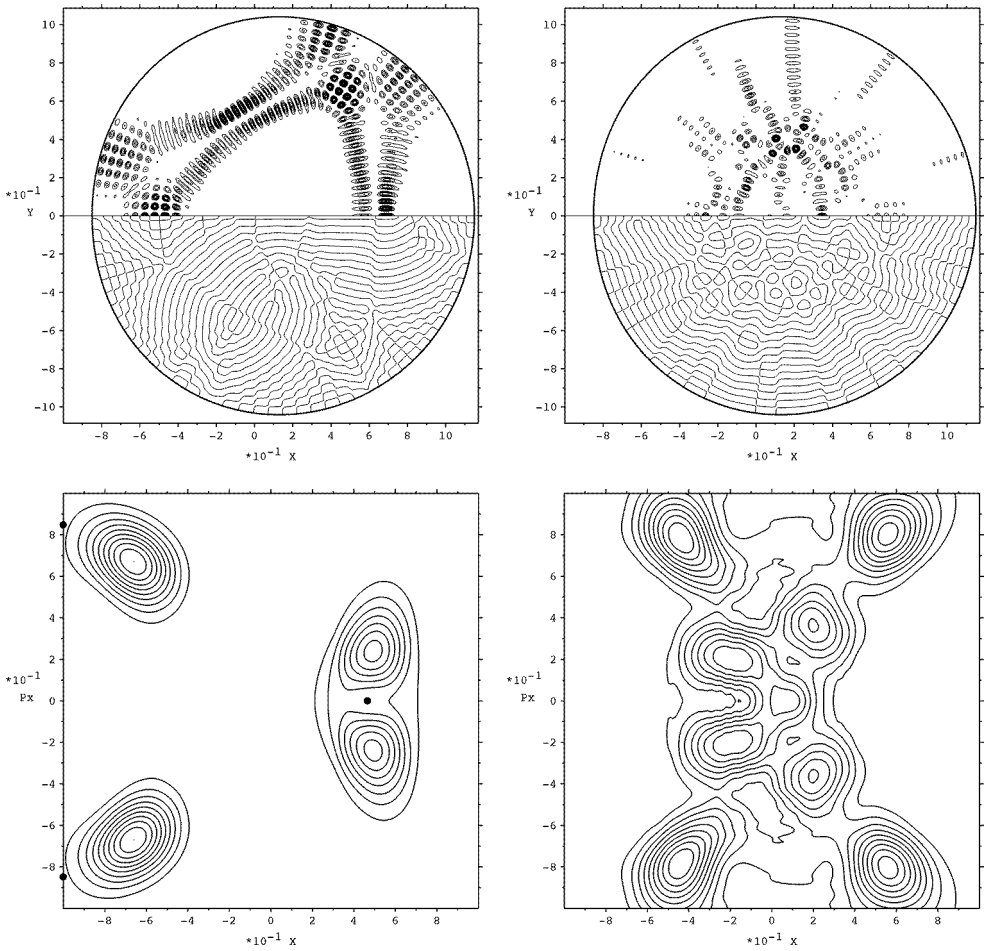

Figure 7. An example of the probability density for a regular (top left) and an irregular (top right) state with the corresponding smoothed projections of their Wigner functions shown below, with the same plotting methods as used in corresponding previous plots. In the phase space plots (bottom row) the x coordinate is shifted by λ as in figure 1. The 'bullets' mark the location of the stable period-three periodic orbit, which is the skeleton of the quantized invariant torus.

Robnik 1998), where each semiclassical eigenstate is spanned by an invariant torus in classical phase space, for which the classical actions are integer multiples of $\overline{h}$ with corrections due to the singularities of projection of the torus onto the configuration space. For fully chaotic systems, and general mixed systems (generic systems), the Gutzwiller periodic orbit theory (Gutzwiller 1990) can, in principle, be employed to obtain the density of states (the spectrum) and the wavefunctions, to the leading semiclassical approximation.

The semiclassical methods cannot, however, predict individual energy levels within a vanishing fraction of the mean level spacing even in the limit $\overline{h} \to 0$ (Prosen and Robnik 1993a, Robnik and Salasnich 1997). This limits their use in the analysis of statistical properties of spectra. Furthermore, in the chaotic case the levels are also very sensitive to perturbations of the system (Percival 1973). The Gutzwiller approach and method is very useful in the qualitative analysis, and in certain contexts also quantitative analysis (in describing the collective and statistical properties), but it is still just the leading term in a certain semiclassical

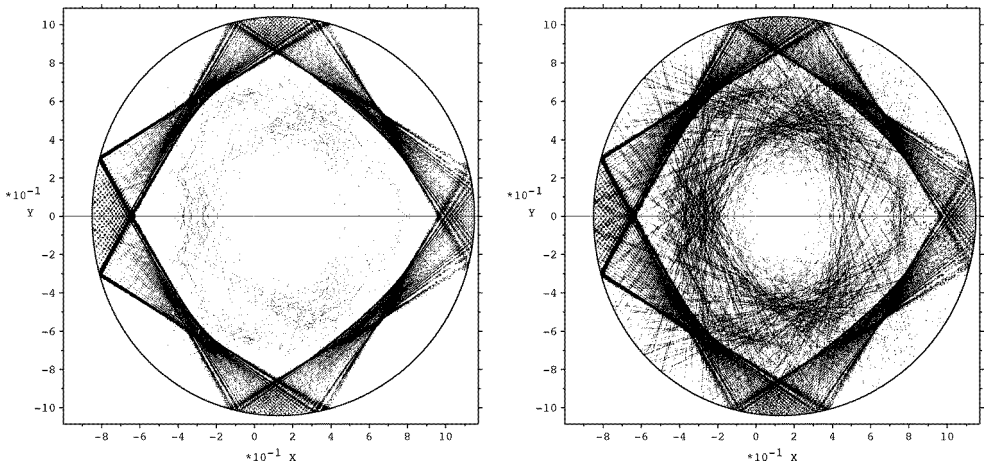

Figure 8. The probability density (16 equally spaced contours from zero to the maximum value) for a pair of close-lying states ($k^2 = 20\,421\,106.7347$, left, and $k^2 = 20\,421\,107.0691$, right) that are superpositions of a regular and an irregular state.

expansion, which is not good enough to resolve the fine structures with sufficient accuracy to make the analysis of *individual states and energy levels* reliable. Therefore, because of the sensitivity of chaotic eigenstates and the approximating nature of the theory, to some extent the questions about the fine structure of individual chaotic states are irrelevant. It is therefore more appropriate to discuss the statistical properties of chaotic states, which are, however, less sensitive to perturbations.

In a mixed system the phase space is divided into chaotic and regular components. Our work was guided by the PUSC (see Robnik 1998), stating that when $\overline{h}$ tends to zero the Wigner function of any eigenstate uniformly condenses on an invariant object in phase space. This can be either a torus in the regular region or a whole chaotic component. Each state could thus be labelled as either regular or irregular (chaotic) in the semiclassical limit. By looking at the catalogue of states at high (and to some extent even at low) energies, one can see that this can indeed be done, though there is still the localization phenomenon present due to the still insufficiently low value of the effective Planck constant.

3.1. Regular states

We start the analysis by considering the regular states. These are the states that can be attributed to quantized tori within the regular regions. For these states we tried to employ the EBK torus quantization. We construct a wavefunction on the torus as a sum of contributions

$$\psi_j(\boldsymbol{q}) = A_j(\boldsymbol{q}) \exp \mathrm{i} \left(\frac{1}{\overline{h}} S_j^{cl}(\boldsymbol{q}) + \phi_j \right) \tag{7}$$

of different projections j of the torus onto configuration space. S_j is the classical action with respect to some point on the torus and A_j^2 the classical density of trajectories on this projection. The phase of the wavefunction must change by an integer multiple of 2π when going around any closed contour of the torus. This gives us the quantization conditions

$$I_i = \frac{1}{2\pi} \oint_{\gamma_i} \boldsymbol{p} \cdot \mathrm{d}\boldsymbol{q} = \overline{h}(n_i + \beta_i/4) \tag{8}$$

where γ_i are the irreducible closed contours on the torus and n_i the torus quantum numbers. The integers β_i are Maslov's corrections and arise due to the changes of phase, ϕ_j, at the singularities of projection of the torus onto configuration space. At each caustic encountered along the contour γ_i the wavefunction acquires a negative phase shift of $\pi/2$, and shifts by π when reflected from a hard wall†. From this consideration it follows that β_i counts the number of caustics plus twice the number of hard walls encountered along the contour.

The main problem arises since, unlike in many completely integrable cases, the transformation to action-angle variables for regular components of mixed-type systems is usually unknown. The object we are dealing with is only the numerically calculated trajectory, so we must make the best of it.

The task of finding the semiclassical EBK wavefunctions can be divided into two parts. The first part involves finding the torus with the desired quantum numbers n_i, the second part being the construction of its appropriate wavefunction in configuration space.

In our billiard system all the regular tori except the whispering gallery ones wind around a stable periodic orbit with a finite number of bounces, l_b. We choose θ_1 to represent the movement of the trajectories along the corresponding periodic orbit while θ_2 represents the winding of the trajectories around it. The Maslov index for the contour along θ_2 is $\beta_2 = 2$ since there are two singularities of projection (caustics) encountered, while for the contour along θ_1 this index is equal to $\beta_1 = 2l_b$. In the case of whispering gallery modes one similarly obtains $\beta_1 = 0$ and $\beta_2 = 3$, if θ_1 is taken along the boundary of the billiard and θ_2 'perpendicular' to it.

We may find the appropriate torus by iteration. We start with a trajectory η in a regular island on the SOS and follow it for a sufficiently long period until it returns to the desired neighbourhood of the initial point, thus approximately completing N_1 integer number of cycles in θ_1 and N_2 in θ_2 in the time T. One can obtain the numbers N_1 and N_2 by knowing the total number of bounces N_b and N_c of the caustics encountered during the process through the topological properties of the torus. For a torus winding around a periodic orbit, $N_1 = N_b/l_b$ and $N_2 = N_c/2$. The winding frequencies on the torus are then given by

$$\omega_i = 2\pi N_i/T. \tag{9}$$

Finding the number of bounces N_b along the trajectory is straightforward. The number of caustics N_c may be obtained by starting a trajectory η' near the original trajectory η on the same torus (more are needed in case of more than two dimensions). Whenever the two trajectories cross there is a singularity of the density of trajectories and hence a caustic.

Of course, one could use the monodromy matrix to find the caustics. There are two reasons for not doing so. The first one is the numerical simplicity of our approach. The more important reason is, however, that if the trajectories η and η' are taken too close together (infinitesimally close together in the monodromy matrix approach) we may observe caustics due to the possible graining of the desired torus into smaller islands of stability, which quantum mechanics is, at the given value of the effective Planck constant, still unable to resolve. A good criterion is that the trajectories should be separated by $\approx 1/n_i$ for each θ_i.

We still have to calculate the action integrals on the torus. The integral along θ_2 can be calculated by the integral

$$I_2 = \frac{1}{2\pi}\oint_{\gamma_2} \boldsymbol{p}\cdot \mathrm{d}\boldsymbol{q} \tag{10}$$

along the curve γ_2 formed by the crossing points of the trajectory with the SOS. This integral is just $1/2\pi$ of the area of the intersection of the torus with the SOS. Another action integral

† If the contour passes the singularity in the contrary direction to that of the Hamiltonian flow on the torus, the phase shifts are of the opposite sign.

we can calculate is the action along the chosen orbit η,

$$I = \frac{1}{2\pi}\int_{\eta} \boldsymbol{p}\cdot \mathrm{d}\boldsymbol{q}. \tag{11}$$

This integral is the sum of $I = N_1 I_1 + N_2 I_2$, so the integral along θ_2 is equal to

$$I_1 = (I - N_2 I_2)/N_1. \tag{12}$$

We must iterate this procedure by choosing different starting points until the proper torus fulfilling the conditions (8) has been found. In general, there are as many conditions as there are degrees of freedom. For two-dimensional billiard systems whose dynamics is independent of energy, all action integrals can be written in the form

$$I_m = G_m\sqrt{E} \tag{13}$$

where G_m is an integral dependent purely upon the geometry of the classical object in question. In order to obtain the correct quantized torus, instead of solving two separate equations, due to this scaling property we only need to find the appropriate ratio of the (geometric) actions:

$$\frac{I_1}{I_2} = \frac{n_1 + \beta_1/4}{n_2 + \beta_2/4}. \tag{14}$$

We used the robust bisection method to fulfil this condition since the dependence of actions upon initial conditions is not smooth due to the previously mentioned graining of the tori. Note that this procedure yields only the correct geometry of the quantized torus, the energy of which must still be determined by the quantization conditions (8).

The classical action as a function of time can then be written as

$$\int_{q_0}^{q(t)} L(\boldsymbol{q},\dot{\boldsymbol{q}})\,\mathrm{d}t = S(t) = (I_1\omega_1 + I_2\omega_2)t \tag{15}$$

so one immediately obtains the semiclassical energy as

$$E = \frac{\partial S}{\partial t} = I_1\omega_1 + I_2\omega_2. \tag{16}$$

In our case we took the quantized values for I_1 and I_2 and took into account that for billiard systems the angular frequencies are of the form

$$\omega_m = \lambda_m\sqrt{E} \tag{17}$$

where λ_m are frequencies dependent again only upon the geometry of the chosen torus.

In principle, one could obtain the semiclassical energy without considering the angular frequencies ω_i by simply finding the appropriate torus through the quantization conditions (8) and reading its energy. In a KAM system such as ours, however, these quantization conditions may be only approximately fulfilled due to the fine structure of the phase space. In contrast to the actions I_i, the frequencies ω_i do not depend as strongly on the initial conditions (typically, close to the main periodic orbit of an island of stability the transversal frequency does not vanish but is characteristic of the periodic orbit). So by taking the quantized values for actions I_i and the numerical values for ω_i in equation (16) the best estimate of the semiclassical energy is obtained.

Once the proper torus has been found, we proceed to the second step. We need to span the semiclassical wavefunction (7) on this torus. Again we only deal with a trajectory, so we must find means of representing the wavefunction with it. We may write the wavefunction in the form

$$\psi_j(\boldsymbol{q}) = \lim_{T\to\infty} 1/T\int_0^T \mathrm{d}t\,\delta(\boldsymbol{q}_{cl}(t) - \boldsymbol{q})D_j(\boldsymbol{q}_{cl}(t))\exp \mathrm{i}\left(\frac{1}{\hbar}S_j(\boldsymbol{q}_{cl}(t) + \phi_j\right) \tag{18}$$

where $\boldsymbol{q}_{cl}(t)$ is the classical trajectory in configuration space. This definition is appropriate only in the sense of integrals of the wavefunction over configuration space. Hence we can determine the function D_j by integrating the wavefunction over a small volume V',

$$\int_{V'} \mathrm{d}V\ \psi_j = \lim_{T\to\infty} D_j(\boldsymbol{q}) \exp \mathrm{i}\left(\frac{1}{\hbar} S_j(\boldsymbol{q}) + \phi_j\right) \frac{T'}{T} \tag{19}$$

where T' is the time the trajectory spends in the volume V'. This time is proportional to the density of trajectories A_j^2 in the volume V',

$$T' = T A_j^2(\boldsymbol{q}) V'. \tag{20}$$

If we want the expression (19) to be consistent with (7),

$$D_j = \frac{1}{A_j} \tag{21}$$

must hold.

We still have to account for the phase shifts when the trajectory traverses from one projection of the torus onto another. This can be done hand in hand with the estimation of the density of trajectories A_j^2. Again, we start a trajectory $\boldsymbol{q}'_{cl}$ close to the original one (more trajectories are needed in more than two degrees of freedom). Once again, we could use the monodromy matrix approach, but the same criticism applies here as in the case of finding the appropriate tori. Let us imagine a bundle of trajectories inside a small parallelogram spanned by the three points $\boldsymbol{q}_{cl}$, $\boldsymbol{q}'_{cl}$ and $\boldsymbol{q}_{cl} + \dot{\boldsymbol{q}}_{cl}\delta t$, where all three points lie on the given torus. The area of the parallelogram is given by the absolute value of

$$\boldsymbol{P} = \dot{\boldsymbol{q}}_{cl} \times (\boldsymbol{q}'_{cl} - \boldsymbol{q}_{cl})\delta t. \tag{22}$$

As we are only interested in the relative sizes of this parallelogram, we may set $\delta t = 1$. The reciprocal value of this area is proportional to the density of trajectories,

$$A_j^2 = \alpha/|P|. \tag{23}$$

The value of α does not change along the trajectory and can be subsequently determined by the normalization of the semiclassical wavefunction. Whenever the value of P changes its sign, the trajectory has encountered a caustic and has passed from one projection, j, of the torus to another one, k. At this point the wavefunction acquires a phase shift

$$\phi_k = \phi_j - \pi/2. \tag{24}$$

The phase shift is equal to π if a hard wall is encountered.

Of course, the construction (18) is, in its original form, unsuitable for numerical computation. We must substitute the δ function in the integral by a function of finite width. The other important reason for doing so is to once again smooth the classical behaviour which can have a far more detailed structure than quantum mechanics can yet resolve. This width does not necessarily need to be isotropic. A good estimate for it is again to be of the order of $1/n_i$ in coordinates θ_i projected onto configuration space.

We used a Gaussian for the wide δ function. If we adjusted the width and the amplitude of the Gaussian so that it followed the classical density of trajectories, a remarkable similarity of our method with that of Heller's wavepacket approach was observed (Heller 1991). There are, however, two important differences. The wavepacket approach starts with a wavepacket with the expected value of energy equal to that of the exact wavefunction and then tries to construct its semiclassical approximation. Our approach is independent of the exact eigenstate. All the information we have to supply is the quantum numbers and the geometrical properties of the (projection of the) torus, obtaining from them both the semiclassical energy (16) and

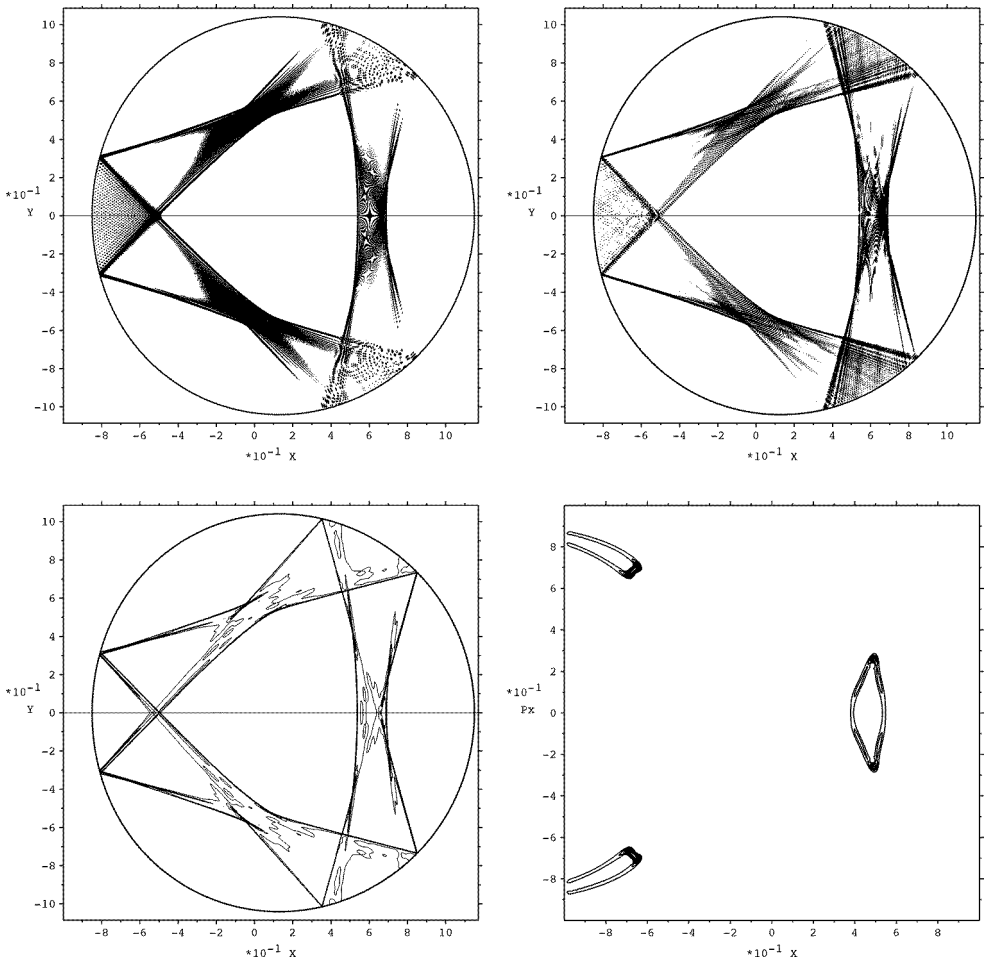

Figure 9. The probability density for a regular state with $k^2 = 20\,420\,831.0603$ (top left), its semiclassical approximation with $k_{sc}^2 = 20\,420\,828.18$ (top right), with the quantum numbers on the torus being $n_1 = 6752$ and $n_2 = 37$ (16 equally spaced contours from zero to the maximum value in both cases). In the bottom row we show the classical density with 20 contours from zero to the maximum of the appropriate torus (left) and the smoothed projection of the exact Wigner function (right), with ten contours from zero to the maximum value. In the phase space plot (bottom right) the x coordinate is shifted by λ as in figure 1.

the wavefunction. The other important difference is that the wavepacket approach relies on the monodromy matrix of the trajectory, the use of which can be questionable for obtaining semiclassical wavefunctions in mixed-type systems due to the fine structure of the classical phase space, as was pointed out before.

We show three examples of the regular states in the figures 9–11. For each of the states we present the exact numerical quantum probability density (top left), the probability density of its semiclassical approximation (top right), the classical density of trajectories on the appropriate torus (bottom left) and the smoothed projection of the exact Wigner function (bottom right). The semiclassical wavefunctions shown are remarkable as they possess all of the features of their exact counterparts that are larger than the appropriate wavelength. Note that for each torus there are two characteristic wavelengths since there are two quantum numbers

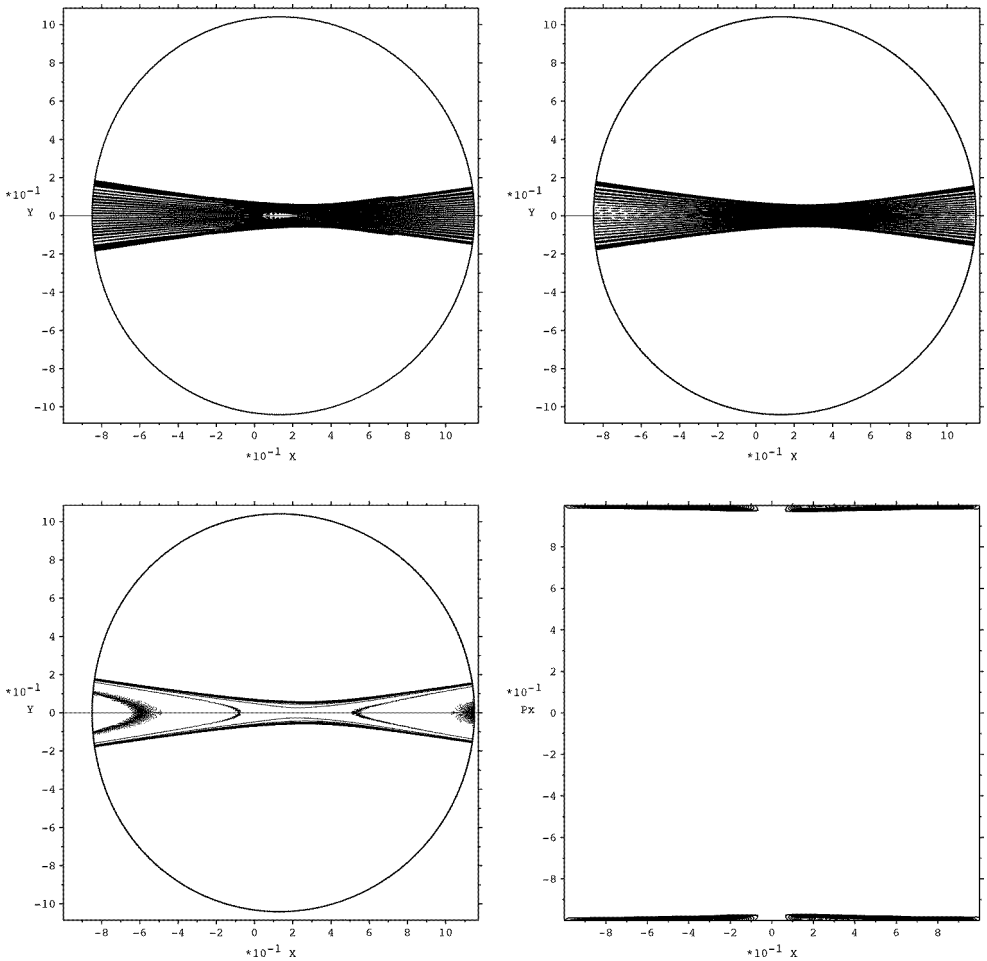

Figure 10. The same as in figure 9 but for the state with $k^2 = 20\,421\,002.7443$ and its semiclassical approximation with $k_{sc}^2 = 20\,420\,999.46$, $n_1 = 2861$ and $n_2 = 20$.

associated with it. As it happens, in our case, the two wavelengths can be of different orders of magnitude.

There were, however, some 'regular' states that we were unable to reproduce semiclassically. The first class of these states can be described as localized chaotic states since their Wigner function clearly shows that they lie in the chaotic region, yet very close to an island of stability, which gives them a regular appearance. The other class are the states whose Wigner transforms lie in the regular regions, but where the primary tori have already been destroyed by the perturbation and now form secondary tori interwoven by small regions of chaotic motion, and even the smoothing of classical dynamics, as described above, fails.

The accuracy of the semiclassical energies that we were able to reproduce may seem remarkable, since the error is approximately 5 units of energy at the energies around 2×10^7. Such accuracy, however, is still insufficient to perform short-range spectral statistics since the mean level spacing in our system is approximately 8 units of energy. This experience is, of course, in agreement with the proposition and conclusion that the semiclassical methods (to the

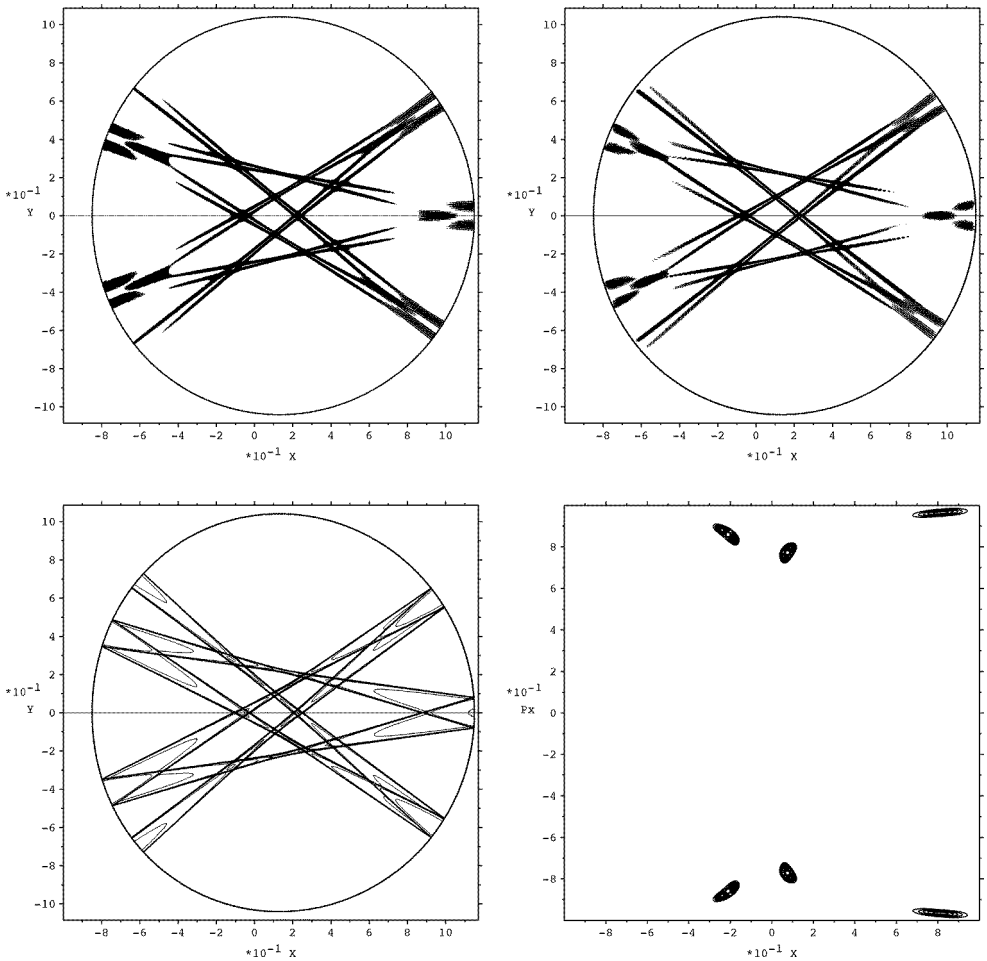

Figure 11. The same as in figure 9 but for the state with $k^2 = 20\,421\,387.1741$ and its semiclassical approximation with $k_{sc}^2 = 20\,421\,385.96$, $n_1 = 8648$ and $n_2 = 1$.

leading order) cannot resolve the energy spectra within the vanishing fraction of the mean level spacing, and also not the structures of the wavefunctions smaller than de Broglie wavelength (Prosen and Robnik 1993a, Robnik and Salasnich 1997).

3.2. Irregular states

While for the regular states it was quite straightforward to find their semiclassical approximations, the nature of irregular states is very different. The chaotic component of a system does not possess any obvious structure. While Gutzwiller's approach can yield the properties of a quantum system by a summation over all periodic orbits of its classical counterpart, the relevance of examining individual chaotic states becomes questionable. These states are very sensitive to small perturbations of the system, so in any physical system the individual features of the states are lost when the effective Planck constant tends to zero. The features that are insensitive to small perturbations are, however, the statistical properties of spectra and eigenstates.

One measure of the statistical properties of the wavefunctions is the wavefunction autocorrelation function,

$$C(\boldsymbol{q}, \boldsymbol{x}) = \frac{\langle \psi^\dagger(\boldsymbol{q}' - \boldsymbol{x}/2)\psi(\boldsymbol{q}' + \boldsymbol{x}/2)\rangle_{\boldsymbol{q}' \in \epsilon(\boldsymbol{q})}}{\langle \psi^\dagger(\boldsymbol{q}')\psi(\boldsymbol{q}')\rangle_{\boldsymbol{q}' \in \epsilon(\boldsymbol{q})}}. \tag{25}$$

The area of averaging $\epsilon(\boldsymbol{q})$ close to the point $\boldsymbol{q}$ should be taken such that its linear size is many wavelengths across, but still small enough that the local properties of classical mechanics within it are largely uniform.

If one takes the Fourier transform of the Wigner function (3), it is easy to show that

$$\int W(\boldsymbol{q}, \boldsymbol{p}) \exp(\mathrm{i}\boldsymbol{p} \cdot \boldsymbol{x}/\overline{h})\, \mathrm{d}^N \boldsymbol{p} = \psi^\dagger(\boldsymbol{q} - \boldsymbol{x}/2)\psi(\boldsymbol{q} + \boldsymbol{x}/2). \tag{26}$$

By knowing the Wigner function of an eigenstate, it is then possible to use this result to calculate its autocorrelation function.

According to the principle of uniform semiclassical condensation, the Wigner function of any chaotic state should uniformly condense on the whole chaotic component when the effective $\overline{h}$ tends to zero. Let us limit ourselves to the cases of the Hamiltonians with an isotropic dependence upon $\boldsymbol{p}$. We can write the semiclassical Wigner function in the form of a conditional δ function

$$W_{\mathcal{D}_i}(\boldsymbol{q}, \boldsymbol{p}) = \alpha\delta(\{\boldsymbol{q}, \boldsymbol{p}\} \in \mathcal{D}_i;\, E - H(\boldsymbol{q}, p)) \tag{27}$$

where $\mathcal{D}_i$ denotes a chaotic component and α is the normalization constant. The Fourier transform (26) of this Wigner function is

$$\int W_{\mathcal{D}_i}(\boldsymbol{q}, \boldsymbol{p}) p^{N-1} \exp(\mathrm{i}\boldsymbol{p} \cdot \boldsymbol{x}/\overline{h})\, \mathrm{d}p\, \mathrm{d}\Omega_p = \alpha \frac{p(\boldsymbol{q})^{N-1}}{\frac{\partial H}{\partial p}(\boldsymbol{q},\, p(\boldsymbol{q}))} \int_{\Omega_p \in \mathcal{D}_i(\boldsymbol{q})} \mathrm{d}\Omega_p\, \exp(\mathrm{i}\boldsymbol{p} \cdot \boldsymbol{x}/\overline{h}) \tag{28}$$

where $p(\boldsymbol{q})$ denotes the absolute value of momentum at the point $\boldsymbol{q}$. The integration over the spatial angle Ω_p is performed along all the directions of momentum that constitute the chaotic component $\mathcal{D}_i$ at the point $\boldsymbol{q}$. The autocorrelation function is then equal to

$$C_{\mathcal{D}_i}(\boldsymbol{q}, \boldsymbol{x}) = \frac{\langle \int_{\Omega_p \in \mathcal{D}_i(\boldsymbol{q}')} \mathrm{d}\Omega_p \exp(\mathrm{i}\boldsymbol{p} \cdot \boldsymbol{x}/\overline{h})\rangle_{\boldsymbol{q}' \in \epsilon(\boldsymbol{q})}}{\langle \int_{\Omega_p \in \mathcal{D}_i(\boldsymbol{q}')} \mathrm{d}\Omega_p \rangle_{\boldsymbol{q}' \in \epsilon(\boldsymbol{q})}}. \tag{29}$$

The averaging area should once again stretch across many wavelengths.

If the chaotic component is equal to the whole energy surface, as is the case in completely ergodic systems, in the case of two degrees of freedom one obtains the well known Berry result (Berry 1977)

$$C_{ergodic}(\boldsymbol{x}) = J_0(p(\boldsymbol{q})r/\overline{h}) \qquad r = |\boldsymbol{x}|. \tag{30}$$

However, when the system is of the mixed type the autocorrelation function ceases to be isotropic and acquires contributions of higher-order Bessel functions. We can obtain these contributions by rewriting the integrals $\int_{\phi_p \in \mathcal{D}_i} f(\phi_p)\, \mathrm{d}\phi_p$ by integrals of the characteristic function $\int \chi_{\mathcal{D}_i}(\phi_p) f(\phi_p)\, \mathrm{d}\phi_p$, where in two degrees of freedom the spatial angle is replaced by a simple angle ϕ_p and $f(\phi_p)$ is an arbitrary function of ϕ_p. If we write the characteristic function as a Fourier series,

$$\chi_{\mathcal{D}_i}(\boldsymbol{q}; \phi_p) = \sum_{m=-\infty}^{\infty} \kappa_m^{\mathcal{D}_i}(\boldsymbol{q}) \exp(\mathrm{i}m\phi_p) \tag{31}$$

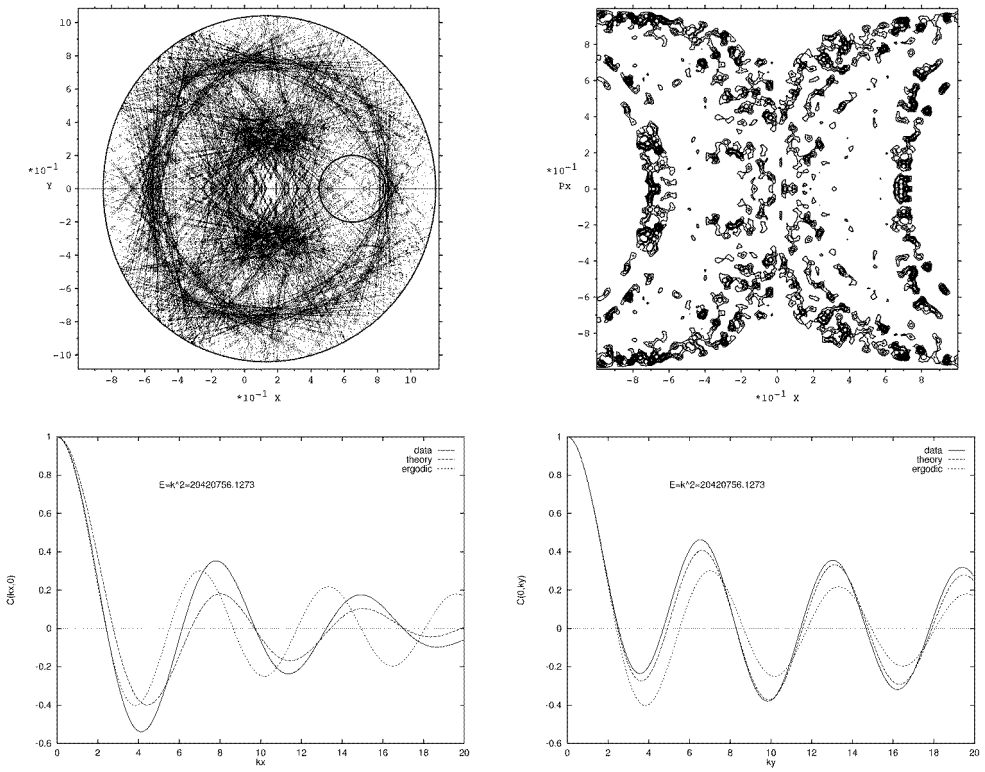

Figure 12. In the top row we show the probability density for the chaotic state with $k^2 = 20\,420\,756.1273$ (left, eight contours) with the smoothed projection of its Wigner function (right, ten contours). The circle of radius 0.2 centred at $x = 0.65$ is the region of averaging. In the phase space plot (top right) the coordinate x is shifted by λ as in figure 1. In the bottom row we plot the wavefunction autocorrelation function (averaged over the small circle as explained in text) in the x (left) and y (right) directions.

it is quite straightforward to show, by using the integral representations of the Bessel functions, that

$$C_{\mathcal{D}_i}(\boldsymbol{q}, \boldsymbol{x}) = \frac{\langle \sum_{m=-\infty}^{\infty} \kappa_m^{\mathcal{D}_i}(\boldsymbol{q}') i^m J_m(p(\boldsymbol{q}')r/\overline{h}) \exp(\mathrm{i}m\phi_x)\rangle_{\boldsymbol{q}'\in\epsilon(\boldsymbol{q})}}{\langle \kappa_0^{\mathcal{D}_i}(\boldsymbol{q}')\rangle_{\boldsymbol{q}'\in\epsilon(\boldsymbol{q})}} \tag{32}$$

where ϕ_x is the polar angle of the vector $\boldsymbol{x}$.

As in the case of the regular states, we cannot numerically deal with components of phase space but with trajectories. So we start a trajectory within the chaotic component $\mathcal{D}_i$ and not the direction of its momentum $\phi_p^j(\boldsymbol{q})$ at each passage j through the neighbourhood of the point $\boldsymbol{q}$. The averaged characteristic function for this neighbourhood can then be represented as

$$\chi_{\mathcal{D}_i}(\boldsymbol{q}; \phi_p)/\kappa_0^{\mathcal{D}_i}(\boldsymbol{q}) = \frac{\sum_{j=1}^{n} d_j \delta(\phi_p - \phi_p^j)}{\sum_{j=1}^{n} d_j} \tag{33}$$

where d_j are the lengths covered by the particle in the averaging neighbourhood at the passage j, and n is the number of passages. One can check that this method tends to the proper angular distribution $\chi_{\mathcal{D}_i}$ as $n \to \infty$ for any shape of the averaging neighbourhood, if one assumes the homogeneity of trajectories at a given angle (which is true for a small enough neighbourhood, over which the classical phase space picture does not vary). For any incident angle ϕ the

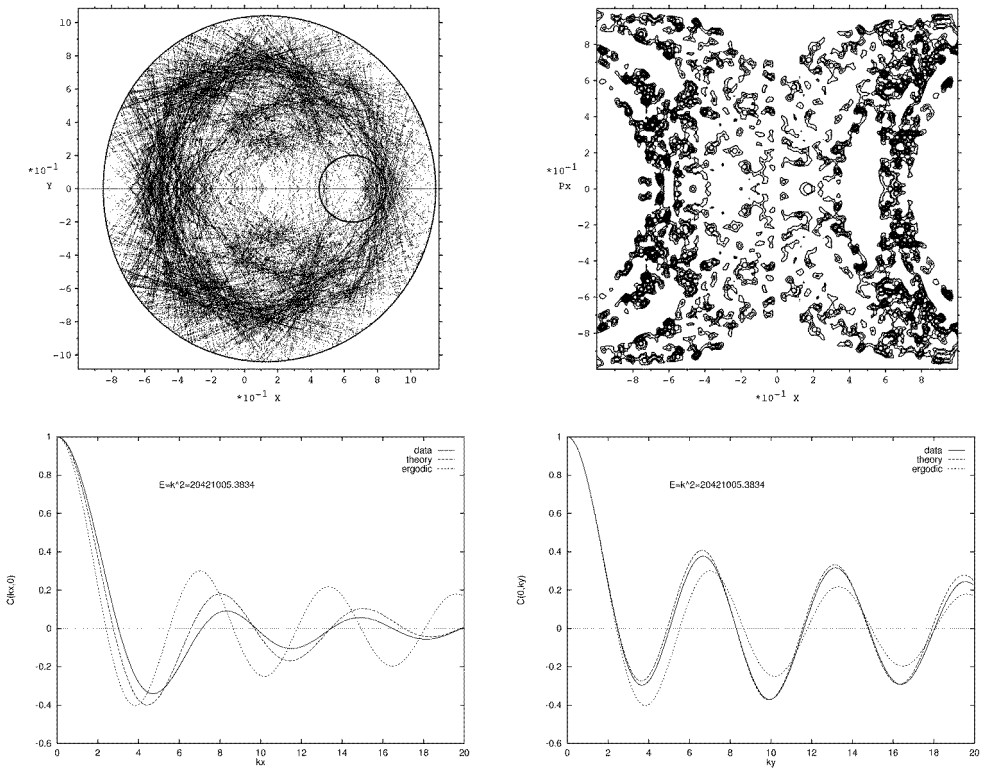

Figure 13. The same as in figure 12 but for the state with $k^2 = 20\,421\,005.3834$.

conditional expected value of a contribution to the equation (33) is proportional to $\int d_j \, \mathrm{d}x$, where x is the homogeneously distributed impact parameter (the direction perpendicular to the incident angle). This integral just gives the area of the averaging neighbourhood and is clearly the same for all incident angles.

If the area of averaging is large enough so that the variations in the classical phase space picture become important, the above procedure is still valid as long as the value of the momentum does not change appreciably (as is the case in our billiard system, where between the bounces the momentum remains constant). One can then imagine the large averaging area as being cut into smaller ones within which the above assumptions still hold true.

We compared the autocorrelation functions for a few chaotic states with the semiclassical prediction in figures 12–14. The averaging area $\epsilon(\boldsymbol{q})$ was taken as a circle of radius 0.2 around the point $(x, y) = (0.65, 0)$ (the coordinates are as defined in equation (1)). It was taken as the same for both the semiclassical prediction and for the numerical results. The averaging radius was taken as quite large in order to reduce the localization properties of the wavefunctions, which are still apparent at the values of effective $\overline{h}$ that we were able to obtain. But, this radius still has to be taken small enough in order to avoid completely smoothing out the classical dynamics. The agreement with the semiclassical prediction is quite good particularly in figure 14. In all cases it clearly deviates from the Berry prediction for fully ergodic systems (30), as it must for mixed systems, and tends towards our semiclassical result. Although in some cases there are amplitude deviations from our

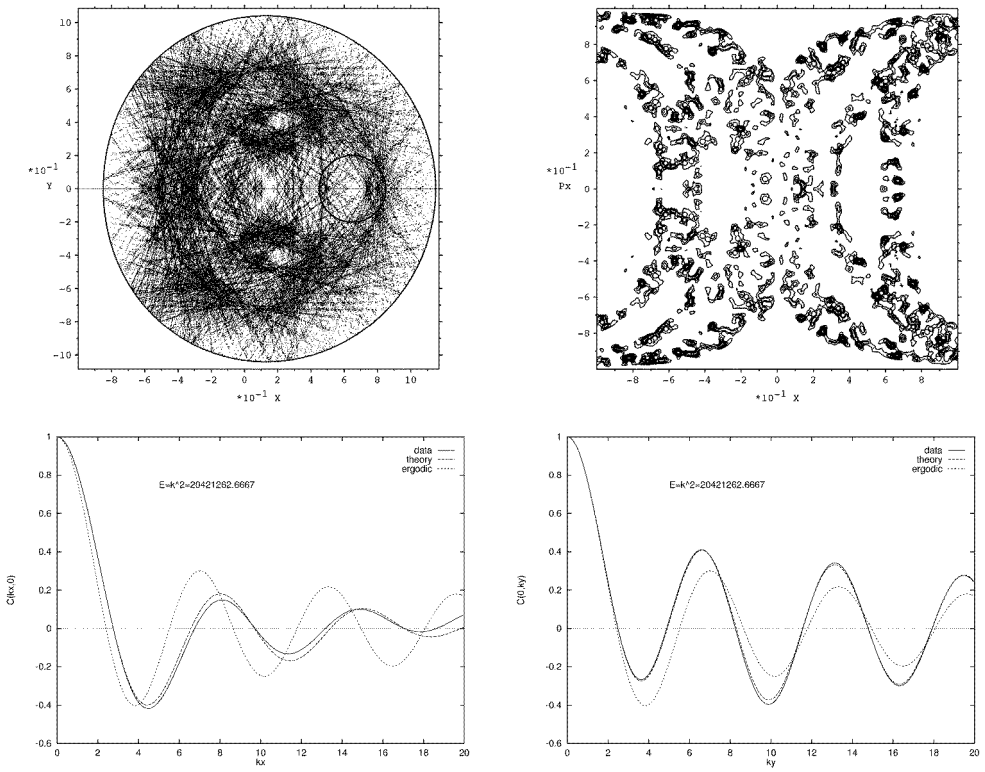

Figure 14. The same as in figure 12 but for the state with $k^2 = 20\,421\,262.6667$.

prediction, in all of the plots the phase of the numerical correlation function matches the phase of its semiclassical prediction and is significantly different from the phase predicted for the fully ergodic case.

4. Discussion and conclusion

As already presented by Prosen and Robnik (1993c), the classification of states into regular and irregular ones is well founded when the effective Planck's constant tends to zero. Its theoretical foundation is the principle of uniform semiclassical condensation of Wigner functions of eigenstates (Robnik 1988, 1998). This separation is not strictly a semiclassical phenomenon since even some of the lowest levels in our catalogue of low-lying states can be classified as either regular or irregular. In the high-energy catalogue of states each state can easily be classified as either chaotic or regular, with only one notable exception, where two close-lying states are a superposition of a regular and an irregular state. These exceptions are expected to disappear with higher energies. While the states can be separated with respect to classical dynamics, the chaotic states in our high-energy catalogue still exhibit the phenomenon of dynamical quantal localization. Their Wigner functions are not uniformly extended over the whole chaotic component, but are only significant on a part of it. This localization is expected to disappear at sufficiently small effective $\overline{h}$, when the quantum mechanical break time $t_{break} = \overline{h}/\Delta E$, where ΔE is the mean level spacing, becomes longer than the time for a typical trajectory to explore the whole chaotic component (diffusion time).

The most important part of this work is, of course, the semiclassical analysis of states. We were able to reconstruct both the semiclassical wavefunction and the semiclassical energy of the regular states by using the EBK quantization. Since our system is of a KAM type, most of the resonant tori are destroyed, forming smaller islands of stability interwoven with chaotic components. The classical mechanics thus shows a rich structure that quantum mechanics, at a fixed value of $\overline{h}$, is still unable to resolve. In order to obtain the regular semiclassical wavefunctions, we had to appropriately smooth out this fine classical behaviour as explained in section 3.1.

We were unable to predict the individual properties of chaotic states. We made a step forward, however, in describing their semiclassical statistical properties. We obtained a semiclassical prediction for the autocorrelation function of their wavefunction, which differs from the one for fully ergodic systems as it is not isotropic. The numerical results confirm this prediction, although there are still localization phenomena at the currently attainable effective $\overline{h}$ that cause deviations from it.

One aspect that needs to be investigated further is the localization properties of the chaotic states. As Casati and Prosen (1998) show in the example of a fully chaotic stadium billiard, in the diffusive regime (ϵ-stadium, having very large ergodic time), the quantum diffusion is halted by the cantori in phase space leading to localization. How these and similar ideas translate to the case of a mixed-type system still remains an open question.

Acknowledgments

We thank Dr Tomaž Prosen for assistance and advice with some computer programs. This work was supported by the Ministry of Science and Technology of the Republic of Slovenia and by the Rector's Fund of the University of Maribor.

References

Berry M V 1977 *J. Phys. A: Math. Gen.* **10** 2083
——1983 *Chaotic Behaviour of Deterministic Systems (Proc. NATO ASI Les Houches Summer School,* ed G Iooss *et al* (Amsterdam: Elsevier) p 171
Berry M V and Robnik M 1984 *J. Phys. A: Math. Gen.* **17** 2413
Berry M V and Wilkinson M 1984 *Proc. R. Soc.* A **392** 15
Bogomolny E 1988 *Physica* D **31** 169
Casati G and Prosen T 1999 *Phys. Rev.* E **59** 2516
Gutzwiller M 1990 *Chaos in Classical and Quantum Mechanics* (Springer: New York)
Heller E J 1984 *Phys. Rev. Lett.* **53** 1515
——1986 *Lecture Notes in Physics* **263** 162
——1991 *Chaos and Quantum Physics (Proc. NATO ASI Les Houches Summer School,* ed M-J Giannoni *et al* (Amsterdam: Elsevier) p 547
Lazutkin V F 1981 *The Convex Billiard and the Eigenfunctions of the Laplace Operator* (Leningrad: Leningrad University Press) (in Russian)
——1991 *KAM Theory and Semiclassical Approximations to Eigenfunctions* (Heidelberg: Springer)
Li Baowen and Robnik M 1994 *J. Phys. A: Math. Gen.* **27** 5509
——1995a *J. Phys. A: Math. Gen.* **28** 2799
——1995b *J. Phys. A: Math. Gen.* **28** 4483
Percival I C 1973 *J. Phys. B: At. Mol. Phys.* **6** L229
Prosen T 1995 *J. Phys. A: Math. Gen.* **28** L349
——1996 *Physica* D **91** 244
——1998 *J. Phys. A: Math. Gen.* **34** 7023
Prosen T and Robnik M 1993a *J. Phys. A: Math. Gen.* **26** L37
——1993b *J. Phys. A: Math. Gen.* **26** 2371
——1993c *J. Phys. A: Math. Gen.* **26** 5365

——1994 *J. Phys. A: Math. Gen.* **27** 8059
——1999 *J. Phys. A: Math. Gen.* **32** 1863
Robnik M 1983 *J. Phys. A: Math. Gen.* **16** 3971
——1984 *J. Phys. A: Math. Gen.* **17** 1049
——1988 in *Atomic Spectra and Collisions in External Fields* ed K T Taylor *et al* (New York: Plenum) pp 251–74
——1989 Bound-state eigenfunctions of classically ergodic Hamilton systems: a theory of scars *University of California, Santa Barbara Preprint* unpublished
——1998 *Nonlin. Phenom. Complex Syst.* **1** 1
Robnik M and Salasnich L 1997 *J. Phys. A: Math. Gen.* **30** 1711
Robnik M and Veble G 1998 *J. Phys. A: Math. Gen.* **31** 4669
Vergini E and Saraceno M 1995 *Phys. Rev.* E **52** 2204
Voros A 1979 *Lecture Notes in Physics* **93** 326